RESEARCH ARTICLE

Yan SU, Fangjun HONG, Lianjie SHU

A building unit decomposition model for energy leakage by infrared thermography image analysis

Abstract A quantitative energy leakage model was developed based on the thermography image data measured for both external and internal building surfaces. The infrared thermography images of both surfaces of doors, windows, and walls of an office building in the Hengqin Campus of University of Macao were taken at various times in a day for four seasons. The transient heat flux for sample units were obtained based on measurements of the seasonal transient local temperature differences and calculations of the effective thermal conductivity from the multiple-layer porous medium conduction model. Effects of construction unit types, orientations, and seasons were quantitatively investigated with unit transient orientation index factors. The corresponding electric energy consumption was calculated based on the air conditioning system coefficient of performance of heat pump and refrigerator cycles for different seasons. The model was validated by comparing to the electric meter records of energy consumption of the air conditioning system. The uncertainties of the predicted total building energy leakage are about 14.7%, 12.8%, 12.4%, and 15.8% for the four seasons, respectively. The differences between the predicted electric consumption and meter values are less than 13.4% and 5.4% for summer and winter, respectively. The typical daily thermal energy leakage value in winter is the highest among the four seasons. However, the daily electric energy consumption by the air conditioning system in summer and autumn is higher than that in winter. The present decomposition model for energy leakage is expected to provide a practical tool for quantitative analysis of energy leakage of buildings.

1 Introduction

Because of the non-contact nature of radiative heat flux based temperature measurements, infrared thermography (IRT) surveys have been applied in temperature measurements in many fields such as electrical device inspection, manufacture malfunction detection, disease diagnostics and building surveys [1–3]. Compared to conventional conduction-based contact measurements, the non-destructive IRT surveys have become more and more popular in building surveys and energy audit [4]. There are different types of building IRT surveys, including heat loss surveys [5], flat roof surveys [6], flood or moisture surveys [7], and structure property surveys [8].

Heat loss surveys of buildings can identify the areas of heat loss, locate the positions of thermal bridge, improve comfort, and identify energy leaks [5–9]. In the early IRT surveys on heat loss of buildings, thermal images of the external surfaces of buildings are taken by the walk-pass method. The images obtained are compared qualitatively with historical images to identify the abnormal thermal energy leakage. Later, walk-through thermography surveys for internal surfaces are also used [10]. However, both walk-pass and walk-through IRT surveys are based on qualitative analysis of thermal images without further quantitative analysis of heat flux based on the two-side temperature distributions.

Quantitative evaluation of thermal bridges in buildings is necessary to satisfy the regulations for energy saving and environment protection [11]. However, direct image analysis on the original images of the whole building to quantify energy leakage is not practical. The reasons are

Yan SU (✉)
Department of Electromechanical Engineering, University of Macao, Taipa, Macao, China
E-mail: yansu@um.edu.mo

Fangjun HONG
School of Mechanical Engineering, Shanghai Jiao Tong University, Shanghai 200240, China

Lianjie SHU
Faculty of Business Administration, University of Macao, Taipa, Macao, China

three-fold. First, the full scale thermal images from IRT surveys on external surfaces of the whole building are not accurate enough for quantitative analysis. This is because the image size has a great impact on the accuracy of heat flux calculations. As shown by Martín Ocaña et al. [12], a scaling of an image to 200% with the same pixel values may cause an error of temperature measurement up to 2°C, which would adversely affect the calculation of heat flux. Second, the thermographic image matching between the original image and the resulting one for energy calculations can easily generate errors. The original whole facade thermography image is a special challenge for thermographic image matching [13]. Image matching needs complex algorithms of scaling, rotation, and translation with many affine deformation parameters such as the tilt angle, incidence angle, and azimuthal angle. Finally, calculations of the local heat flux distributions of a whole building in the image pixel length scale need huge computational costs.

To quantify the energy leakage with local parameter effects, a convective heat flux evaluation method has been developed based on the thermography images taken from external surfaces of a building [14]. Hypothesized constant heat convection coefficients and air temperature are used to estimate convective heat flux. The convective heat flux obtained is used to present the thermal leakage through the thermal bridges corresponding to the building constructions [15]. Inversely, the overall heat transfer coefficient for a piece of building envelope can be estimated [16,17]. However, this type of convective heat flux evaluation method may suffer from large estimation errors due to the assumption of constant heat convection coefficient. The estimation accuracy critically depends on the temperature difference between outside air and sky, which varies to a great extent with unpredictable transient weather conditions [18]. Another limitation with this method is the difficulty in identifying the correct reference convective airflow temperature in the whole building.

To precisely calculate the local effective thermophysical properties of building structures, artificial energy sources have been introduced in the active IRT survey to detect the structure properties [19–21]. Compared to the passive one, which only uses natural or normal energy sources, the active IRT survey has the advantage that under surface properties of structures can be obtained by the transient time series analysis. Combined with transient theoretical analysis methods or multi-dimensional computational methods, the structure thermal properties can be shown in two-dimensional and even in three-dimensional formats by matching the transient predicted with measured results [22–24]. Despite the high accuracy, the active IRT method has a critical shortage of huge computational costs as it requires time-consuming iterations for matching the two or three dimensional temperature fields in mesh scale to measured results. Hence, this method is usually used for a small volume of building materials, at most a piece of limited size of building element [25].

The building IRT surveys can be grouped based on survey objectives, image analysis methods, survey surface positions, and energy sources, which are shown in Fig. 1. Each type can be further divided into two sub-categories. The previous studies mainly fall into two streams: the stream with passive single-side qualitative energy transport survey, and the stream with active double-side quantitative structure detection for a small piece of building elements. The first stream lacks quantitative energy calculations while the second cannot provide the whole building scale information. Besides, there is a lack of a model to correlate the small element quantitative results with the whole building transient energy leakage with effects of different construction elements, orientations, and seasons.

The above limitations motivate the present study to build a more accurate and practical energy leakage model. The proposed model employs a decomposition approach to take the effects of different construction unit types, orientations, and seasons into account. For the sake of simplicity, it is referred to as the seasonal unit decomposition model. Based on the decomposition, the proposed model can accurately calculate both transient local thermal leakage and global energy leakage. Instead of using one global whole external surface thermal image, it estimates the energy leakage based on the transient local heat flux between the external and internal surfaces of building units through image analysis on the coordinates matched temperature distributions of both sides. Challenges of the present model include the effective decomposition of the whole building elements into limited types and numbers of sample units, the accurate transformation of the global and local coordinates for the external and internal side surface thermal images, and the simultaneous measurement of transient pictures in different days and different seasons. In addition, a large number of data sets have to be analyzed systematically with accurate computational codes.

2 Decomposition of the building into construction units

In the present paper, the energy leakage of one office building in the Hengqin Campus of University of Macao, China is investigated. Some views of the office building are shown in Fig. 2. As shown in Fig. 2(a), this building is a four-floor office building with the top layer partially covered with shading roofs. The top layer serves as a natural ventilation sunroom based on the gazebo style design. Air conditioning systems are installed to maintain the indoor environment for the closed domain of the four floors of office rooms. Hence, the closed office domain is considered as the internal domain of the building. Only the external surfaces of the closed domain are considered as
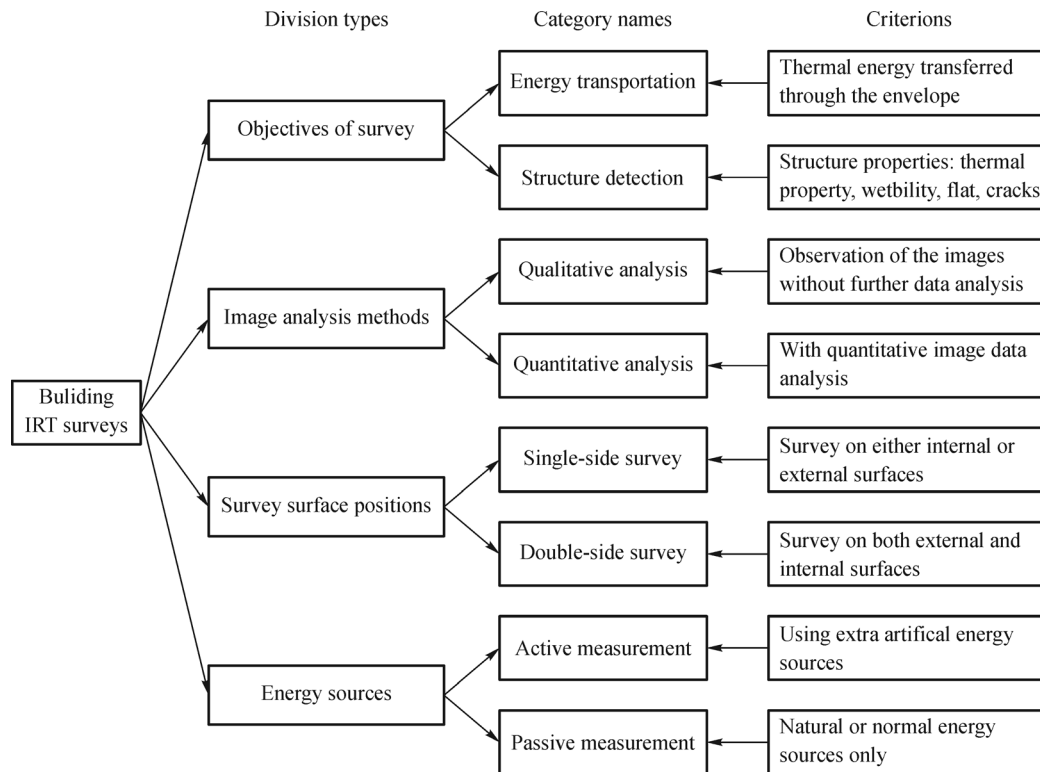
Division types   Category names   Criterions

```
                                   ┌──────────────────┐   ┌──────────────────────────┐
                              ┌───→│ Energy            │←──│ Thermal energy transferred│
                              │    │ transportation    │   │ through the envelope      │
           ┌───────────────┐  │    └──────────────────┘   └──────────────────────────┘
        ┌─→│ Objectives of │──┤    ┌──────────────────┐   ┌──────────────────────────┐
        │  │ survey        │  └───→│ Structure detection│←──│ Structure properties: thermal│
        │  └───────────────┘       └──────────────────┘   │ property, wetbility, flat, cracks│
        │                                                 └──────────────────────────┘
        │  ┌───────────────┐       ┌──────────────────┐   ┌──────────────────────────┐
        │  │               │  ┌───→│ Qualitative analysis│←─│ Observation of the images │
        │  │ Image analysis│──┤    └──────────────────┘   │ without further data analysis│
        ├─→│ methods       │  │    ┌──────────────────┐   └──────────────────────────┘
┌────────┐ └───────────────┘  └───→│ Quantitative analysis│←│ With quantitative image data│
│Buliding│                         └──────────────────┘   │ analysis                  │
│IRT     │─┤                                               └──────────────────────────┘
│surveys │ ┌───────────────┐       ┌──────────────────┐   ┌──────────────────────────┐
└────────┘ │ Survey surface│  ┌───→│ Single-side survey │←─│ Survey on either internal or│
        ├─→│ positions     │──┤    └──────────────────┘   │ external surfaces         │
        │  └───────────────┘  │    ┌──────────────────┐   └──────────────────────────┘
        │                     └───→│ Double-side survey │←─│ Survey on both external and│
        │                          └──────────────────┘   │ internal surfaces         │
        │  ┌───────────────┐       ┌──────────────────┐   └──────────────────────────┘
        │  │               │  ┌───→│ Active measurement │←─│ Using extra artifical energy│
        └─→│ Energy sources│──┤    └──────────────────┘   │ sources                   │
           └───────────────┘  │    ┌──────────────────┐   └──────────────────────────┘
                              └───→│ Passive measurement│←─│ Natural or normal energy  │
                                   └──────────────────┘   │ sources only              │
                                                          └──────────────────────────┘
```

Fig. 1 Classifications of building IRT surveys based on survey objectives, image analysis methods, survey surface positions, and energy sources.

the external thermal energy leakage surfaces. Figure 2(b) shows thermal images of the underlying building taken by a thermal image camera to obtain the temperature distributions. Figure 2(c) shows the horizontal dimensions of the building as well as the direction orientations. This office building is located in Macao with a latitude of 22°11′ N and a longitude of 113°32′ E. The analysis can be used to represent the energy leakage model for a typical office building in south China.

To obtain accurate results, the full facade thermography image with the large length scale should not be used directly for energy calculations. If the whole face picture of the building is directly used to estimate the energy leakage, the error will be large due to limitations of the thermal image resolutions and different distances of different positions to the camera. For example, in Fig. 2(b), the external surface of the windows glasses in the west is a little bit lower than those in the east, due to the differences in the distance of the windows to the camera. Besides, the reflection of the south face plate on the right-hand side of Fig. 2(b) shows a much higher temperature than the building surface facing east. Instead of analyzing the whole external facade thermography image, the transient element scale thermal images are locally captured for each building construction element unit.

In the present paper, the building construction elements are divided into three types: the door, window, and wall

units. Figures 3(a) and 3(b) show the light photos and surface dimensions for the three units, respectively. Figure 3(c) plots the components and thickness dimensions of the building structure unit along the primary heat transfer direction. Now that the top layer serves as a natural ventilation sunroom, the top layer floor, i.e., the roof of the fourth-floor office rooms, will be treated as top flat wall units with equal weights in all orientations.

3 Energy leakage model based on construction units

The survey in the present paper belongs to passive double-side quantitative energy transport surveys, which is different from the existing quantitative building surveys. Different from one-sided external surface surveys that require a lot of environmental parameters based on convection calculations, this survey, based on the conduction through the building envelope, does not require environmental airflow parameters. Besides, unlike the previous quantitative two-side surveys which often analyzes a small piece of building elements, his survey will perform a global quantitative double-side survey with transient image data for various times, seasons, orientations, and building elements. The present model is improved by introducing three quantitative calculations.
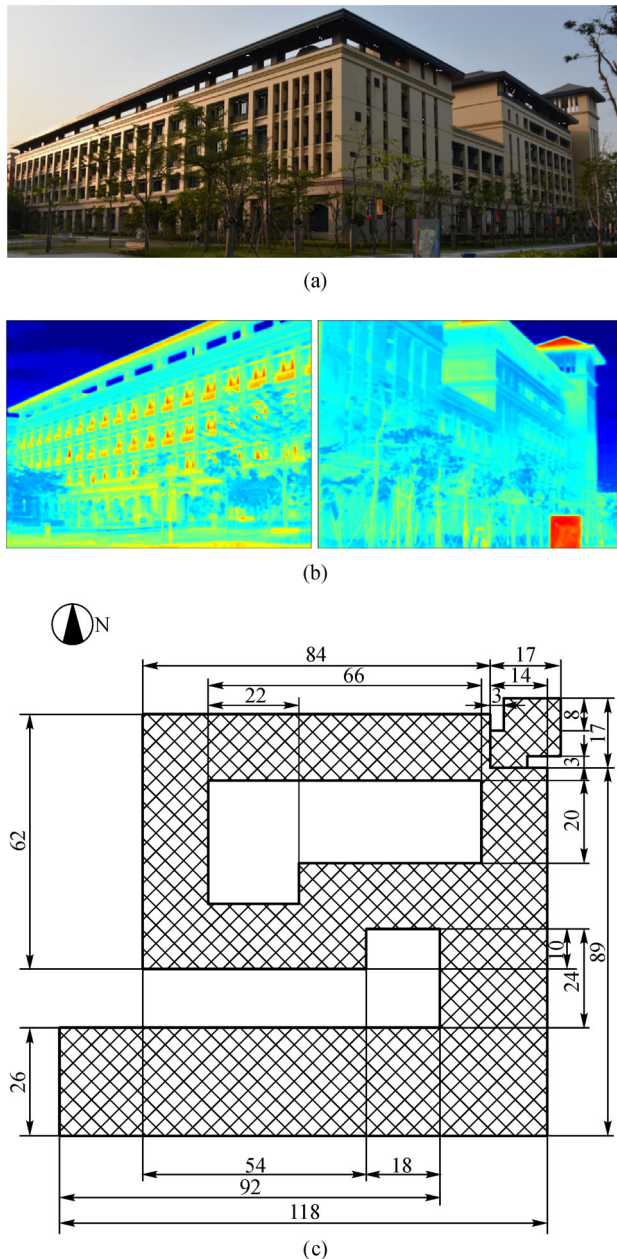
Fig. 2 The global views of the studied office building.
(a) Light photo for the south east outside view; (b) thermal images from the south and east outside views; (c) plot of the horizontal dimensions (m).

The first is the calculation of local structure properties for each type of construction units with multiple-layer porous medium model. The second is the calculation of the local temperature difference distributions based on precisely matched local coordinates of both external and internal surfaces for each type of construction units. The third is the thermal energy flux seasonal orientation index calculation, which is based on the analysis of IRT data in all orientations and seasons.

To quantitatively calculate the energy loss due to the heat flux between the external and internal surfaces of the building, the thermal coefficient for each unit should be calculated first. Then the external and internal surface temperatures for each sample unit in all directions are measured, and the corresponding temperature differences are calculated. The heat flux entering the building through a similar unit in that direction can be calculated based on the product of the temperature difference and the effective thermal resistance of that unit. In this paper, a positive global heat flux means thermal energy gains from the environment, while a negative global heat flux means thermal energy loss to the environment. For the air conditioning system, positive heat flux represents energy leakage for refrigerator cycles, and negative heat flux represents energy leakage for heat pump cycles.

At first, the distributions of the local effective heat conductivity, thermal resistance, and heat coefficient for the three types of units are modeled based on series thermal resistances of multiple porous material layers. For each porous material layer of each unit shown in Fig. 3(c), the porous material layer conductivity k_{layer} can be approximated based on the layer porosity ϕ_{layer}. For each unit in a two-dimensional local coordinate (shown in Fig. 3), the effective thermal conductivity on a local position of $k_e(x, y)$ with multiple layers of porous mediums can be obtained as

$$k_e(x,y) = \cfrac{1}{\sum_{\text{layer}=1}^{\text{lay}_{\max}} \cfrac{L_{\text{layer}}(x,y)/L_u(x,y)}{(1-\phi_{\text{layer}})k_{\text{solid}}(x,y) + \phi_{\text{layer}}k_{\text{air}}(x,y)}},$$
(1)

where L_{layer} and L_u are the thickness of that material layer and the unit on the local coordinate (x, y). Here k_{solid} and k_{air} are the heat conductivity for pure solid material and air encapsulated in pores, respectively. The thermal conductivity of each material used in the present paper is listed in Table 1 [26–29]. The corresponding thermal conduction resistance per unit area and the local heat conduction coefficient $U_e(x, y)$ can be calculated as

$$U_e(x,y) = \frac{1}{R_e(x,y)} = \frac{k_e(x,y)}{L_u(x,y)}$$

$$= \cfrac{1}{\sum_{\text{layer}=1}^{\text{lay}_{\max}} \cfrac{L_{\text{layer}}(x,y)}{(1-\phi_{\text{layer}})k_{\text{solid}}(x,y) + \phi_{\text{layer}}k_{\text{air}}(x,y)}}.$$
(2)

Secondly, the heat flux through local position (x, y) at time t can be calculated based on the local heat conduction coefficient and temperature differences between the internal and external surfaces, given by

$$\dot{q}(x,y,t) = k_e(x,y)\frac{\Delta T(x,y,t)}{L_u(x,y)} = \frac{\Delta T(x,y,t)}{R_e(x,y)}$$
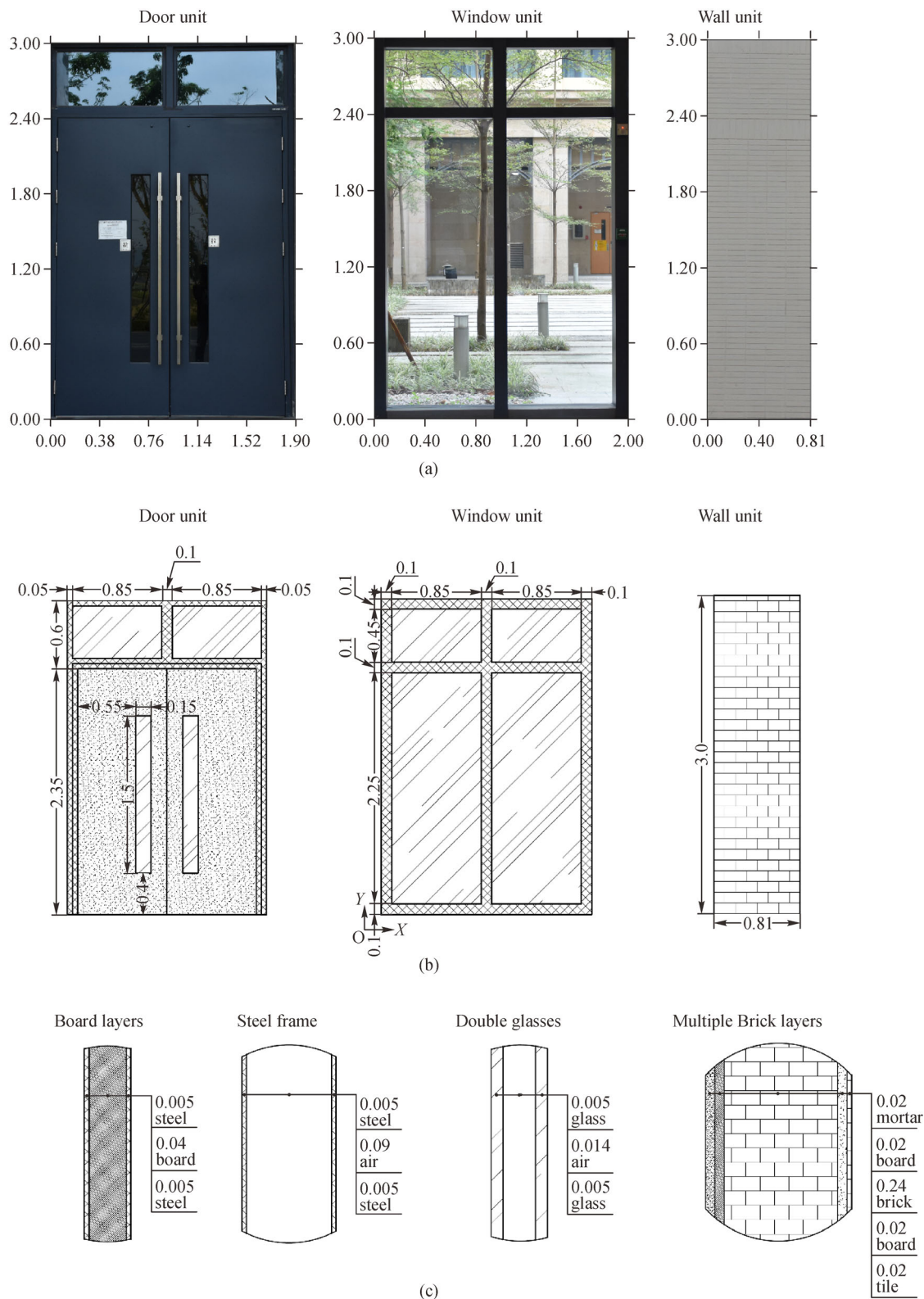
$$= U_e(x,y)\Delta T(x,y,t),$$
(3)

Fig. 3 Photos and dimension samples for three types of units.
(a) Light photos for the three units in form of door (left), window (middle), and wall (right); (b) dimensions of the units (m); (c) dimensions of components in the thickness direction.

Table 1　Thermal conductivity of reference materials

Reference material	Air	Brick	Steel	Glass	Cement-lime	Sand-cement	Ceramic tile	Perlite insulation
Conductivity/(W·(m·K)$^{-1}$)	0.024	0.58	19.0	1.05	0.93	0.9	1.99	0.027

where the transient temperature differences, $\Delta T(x, y, t) = T_{ex}(x, y, t) - T_{in}(x, y, t)$, are calculated based on the matching of local coordinates of external and internal surfaces. The total heat flux through each unit can be obtained by

$$\dot{Q}_u(t) = \int_0^{y_{max}} \int_0^{x_{max}} U_e(x,y)\Delta T(x,y,t)\mathrm{d}x\mathrm{d}y. \qquad (4)$$

This integration is computed based on the space steps in the length scale equivalent to the scale of the thermal image pixel. The total thermal energy leakage during the working hours $[t_{start}, t_{off}]$ can be obtained as

$$Q_{u,\mathrm{Day}} = \int_{t_{start}}^{t_{off}} \dot{Q}_u(t)\mathrm{d}t. \qquad (5)$$

Note that t_{start} = 7:30 am and t_{off} = 18:00 pm are selected as the major working period for the present study based on the historical record of the power usage in a day. This choice is also consistent with the power usage record of Menezes et al. [30]. The electrical power and energy are calculated by

$$P_u(t) = \frac{|\dot{Q}_u(t)|}{\mathrm{COP}(T_{en},t)\eta_\mathrm{p}(t)}, \qquad (6)$$

$$E_{u,\mathrm{Day}} = \int_{t_{start}}^{t_{off}} P_u(t)\mathrm{d}t, \qquad (7)$$

where $\mathrm{COP}(T_{en}, t)$ is the transient coefficient of performance of the air conditioning system at the environment air temperature T_{en}, and $\eta_\mathrm{p}(t)$ is the transient efficiency of the pump system. Note that the COP value in winter is about one larger than that in summer due to the reversed operation of heat pumps or refrigerator cycles of the air conditioning system. The electrical energy consumption values for winter and summer are different, given the same temperature difference.

Thirdly, the thermal energy leakage for one unit can be calculated based on the ratio of the thermal energy leakage through this unit over the sample unit in sample direction. The orientation index factor $r_{u,d,k}(t)$ is defined as the ratio of the unit heat flux to the heat flux through sample unit of the same type,

$$r_{u,d,k}(t) = \frac{\dot{Q}_{u,d,k}(t)}{|\dot{Q}_{u,d_N}(t_N)|}, \qquad (8)$$

where d is the direction index, u is the unit type index, and k is the number index of the same type of units in the same direction. In this paper, d (d = 1, 2, 3, 4, 5) represents the west, east, north, south, and roof top orientation directions,

respectively. The door, window, wall, and roof units are represented by u (u = 1, 2, 3, 4), respectively.

Denote d_N and t_N as the reference direction and time, which are set as north and 13:30 pm in the present paper. The absolute value of $|\dot{Q}_{u,d_N}(t_N)|$ is selected so that the sign of index factors can represent thermal flux directions. The north direction is selected as the reference direction because the external surfaces facing north get less direct solar irradiance compared to those facing the other directions. Hence the heat flux thorough units facing the north more directly reflects the effects of atmosphere temperature change. The time 13:30 is selected as the reference time because the maximum positive heat flux usually appears at this time, due to the maximum atmosphere temperature in a day. Besides, the measured sample units in different orientations have different values of orientation index factors, compared to the heat flux for the same unit type in the reference direction (north) and time (13:30). To simplify the direction factors at different positions in the same direction, it is assumed that

$$r_{u,d,k}(t) = r_{u,d}(t).$$

Hence only one orientation index factor is required for each unit type at each time, defined as

$$r_{u,d}(t) = \frac{\dot{Q}_{u,d}(t)}{|\dot{Q}_{u,d_N}(t_N)|}. \qquad (9)$$

For the sample unit, the orientation index factor in the reference direction at the reference time is set to be one for all unit types, i.e., $r_{u,d_N}(t_N) = 1$. Based on the transient orientation index, the daily averaged orientation index factor in direction d can be obtained as

$$\overline{r}_{u,d} = \frac{\int_{t_{start}}^{t_{off}} r_{u,d}(t)\mathrm{d}t}{\int_{t_{start}}^{t_{off}} \mathrm{d}t}. \qquad (10)$$

In the present paper, $r_d(t)$ is obtained by using image data analysis based on the transient measurement of sample units in all directions.

Finally, the thermal energy leakage for the whole building can be obtained by summing up the leakage of all units in all orientation directions. The whole day heat flux $Q_{u,d,\mathrm{Day}}$ can be obtained by the integration with respect to time as

$$Q_{u,d,\mathrm{Day}} = N_{u,d}\int_{t_{start}}^{t_{off}} \frac{r_{u,d}(t)}{r_{u,d_S}(t)}\dot{Q}_{u,d_S}(t)\mathrm{d}t, \qquad (11)$$

where $N_{u,d}$ is the unit number for the type index u in direction d. When the areas of units are not equal to the sample unit area, $N_{u,d}$ can be approximated as $N_{u,d} = \sum_{k=0}^{k_{max}} A_{u,d,k}/A_{u,d_S}$. According to Eq. (4), the heat flux through the whole sample unit indexed by u in the sample direction d_s can be expressed as

$$\dot{Q}_{u,d_S}(t) = \int_0^{y_{max}} \int_0^{x_{max}} U_{e,u}(x,y)\Delta T_{u,d_S}(x,y,t)\mathrm{d}x\mathrm{d}y. \quad (12)$$

The thermal energy transferred by the sample unit during the working hours $[t_{start}, t_{off}]$ can be obtained by time integration as

$$Q_{u,d_S,Day} = \int_{t_{start}}^{t_{off}} \dot{Q}_{u,d_S}(t)\mathrm{d}t. \quad (13)$$

Hence, for the whole building, the whole day thermal energy leakage can be calculated by

$$\begin{aligned} Q_{B,Day} &= \sum_{d=1}^5 \sum_{u=1}^4 N_{u,d} \int_{t_{start}}^{t_{off}} \frac{r_{u,d}(t)}{r_{u,d_S}(t)} \dot{Q}_{u,d_S}(t)\mathrm{d}t \\ &\approx \sum_{d=1}^5 \sum_{u=1}^4 N_{u,d} \left(\frac{\overline{r}_d}{\overline{r}_{d_S}}\right) Q_{u,d_S,Day}, \end{aligned}$$

(14)

where $r_{u,d_S}(t) = \dot{Q}_{u,d_S}(t)/|\dot{Q}_{u,d_N}(t_N)|$ is defined in Eq. (9). Considering the air leakage from door and windows, the thermal energy leakage ratio due to air flow is represented by $\overline{r}_{u,al}$ ($u = 1,2$). Hence, the total thermal energy leakage can be estimated by

$$\begin{aligned} Q_{Ball,Day} &\approx \sum_{d=1}^5 \sum_{u=1}^4 N_{u,d} \left(\frac{\overline{r}_{u,d}}{\overline{r}_{u,d_S}}\right) Q_{u,d_S,Day} \\ &\quad + \sum_{d=1}^2 \sum_{u=1}^4 N_{u,d} \left(\frac{\overline{r}_{u,al}}{\overline{r}_{u,d_S}}\right) Q_{u,d_S,Day}. \quad (15) \end{aligned}$$

The first term on the right-hand side of Eq. (15) refers to the thermal energy leakage due to conduction, while the second term refers to the thermal energy leakage due to convection. In the present energy ratio index model, sample unit area integration and time integration are performed. The unit in any type and any direction of the building are calculated based on the sample unit values adjusted with unit direction indexes. The present model reduces the huge numbers of integrations based on the image pixel scale, but it still includes effects of different unit thermal properties and different orientations.

The whole day electric energy consumption due to the thermal energy leakage is

$$E_{Ball,Day} \approx \frac{\sum_{d=1}^5 \sum_{u=1}^4 N_{u,d} \left(\frac{\overline{r}_{u,d}}{\overline{r}_{u,d_S}}\right) Q_{u,d_S,Day} + \sum_{d=1}^2 \sum_{u=1}^4 N_{u,d} \left(\frac{\overline{r}_{u,al}}{\overline{r}_{u,d_S}}\right) Q_{u,d_S,Day}}{\overline{COP}(\overline{T}_{en,Day})\overline{\eta}_{p,Day}}, \quad (16)$$

where $\overline{COP}(\overline{T}_{en,Day})$ and $\overline{\eta}_{p,Day}$ are the time averaged coefficient of performance of the air conditioning system and efficiency of the pump system in that day. Similarly, $\sum_{d=1}^5 \sum_{u=1}^4 N_{u,d} \left(\frac{\overline{r}_{u,d}}{\overline{r}_{u,d_S}}\right) Q_{u,d_S,Day}/\overline{COP}(\overline{T}_{en,Day})\overline{\eta}_{p,Day}$ in Eq. (16) represents the electric energy consumption due to thermal leakage caused by conduction, and the rest term $\sum_{d=1}^2 \sum_{u=1}^4 N_{u,d} \left(\frac{\overline{r}_{u,al}}{\overline{r}_{u,d_S}}\right) Q_{u,d_S,Day} / \overline{COP}(\overline{T}_{en,Day})\overline{\eta}_{p,Day}$ represents the electric energy consumption due to thermal leakage caused by convection.

4 Results

4.1 Thermal property distributions of sample units

The distributions of sample unit effective thermal properties of heat conductivity k_e, thermal resistance R_e, and heat coefficient U_e are plotted in Figs. 4(a) to 4(c), respectively. The left, middle, and right columns of Fig. 4 show the thermal properties of a sample unit corresponding to door, window, and wall, respectively.

From the door unit k_e distributions shown in Fig. 4 (a), it can be observed that the effective heat conductivity of the major wood board part is less than 0.2 W/(m·K). The k_e of the single layer glass part of the door unit is about 1.0 W/(m·K), which is higher than that of the metal frame part of 0.4 W/(m·K). From the window unit k_e distributions, it can be seen that the double glass part of the window unit has a lower k_e compared to the metal frame part. The wall unit has a relatively uniform distributed k_e of about 0.25 W/(m·K).

The heat resistance per unit area of each sample unit (Fig. 4 (b)) clearly shows the difference of the thermal property for the three types of units. Note that the overall heat conduction coefficient U_e is the inverse of R_e. As can be seen from Fig. 4(c), when the temperature difference is $\Delta T = 1$ K, the heat flux through the single glass part of the door is as high as 220 W/m², about 190 W/m² through steel frames, and is less than 30 W/m² through the board part of door and double glass of window. The distributions shown in Fig. 4(c) will be combined with the further measured temperature difference distributions between external and internal surfaces for more precise calculations of heat flux through the building envelope.

4.2 Transient temperature distributions of sample units

With the computational code developed in software Matlab, the thermal image data are analyzed and plotted
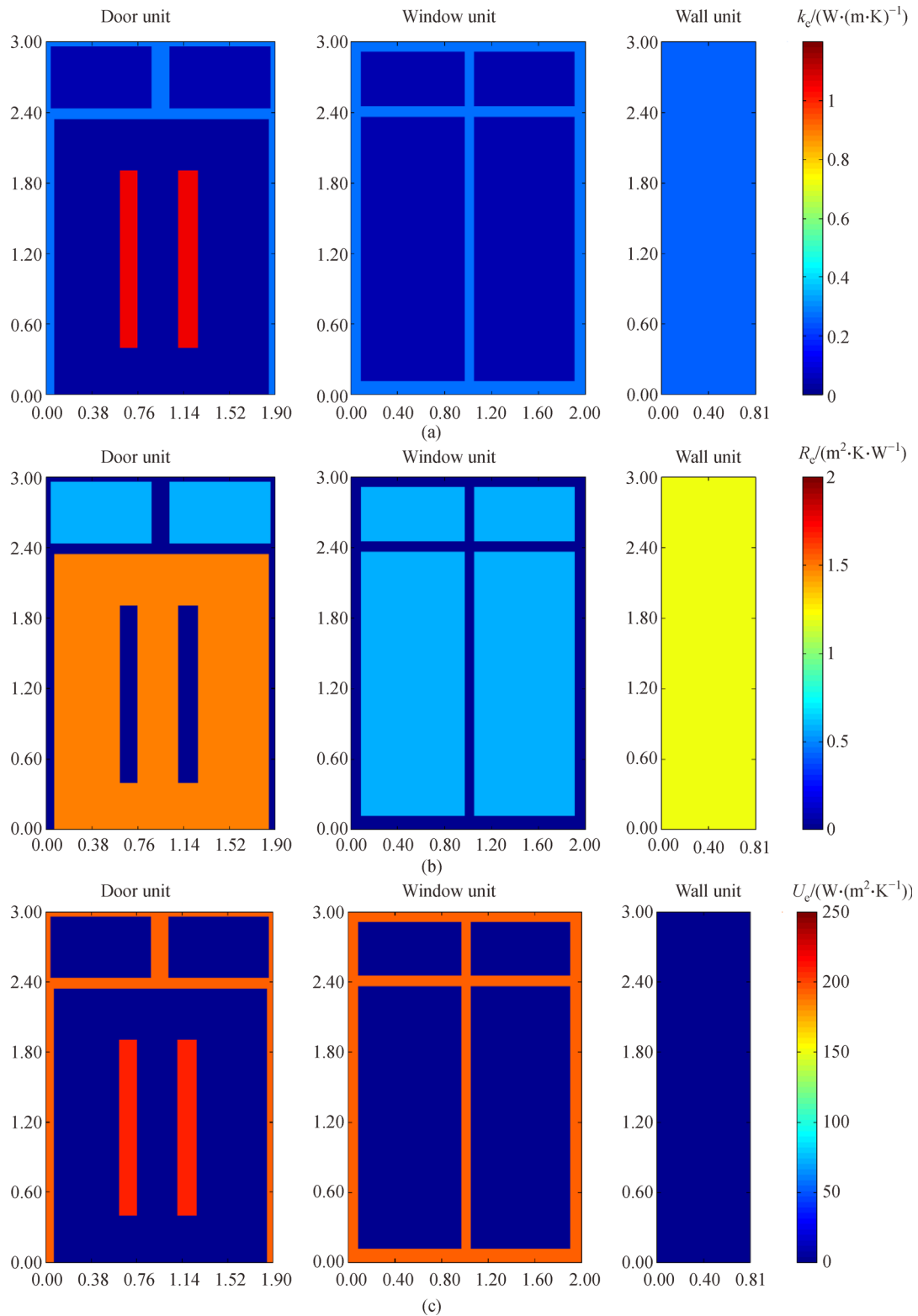
Fig. 4 Effective thermal conductivity and thermal resistance distributions of the three units.
(a) Effective thermal conductivity; (b) effective thermal resistance; (c) local heat conduction coefficient.

based on local coordinates starting from the left bottom corner of the external surface of the units. The measured temperature distributions of both the external and internal surfaces for the three construction units at 12:00 on October 19, 2017 are demonstrated in Figs. 5(a) and 5(b), respectively. As can be seen from Fig. 5(a) that the maximum external surface temperatures for the door, window, and wall units are (37.3±0.5)°C, (27.6±0.5)°C, and (30.4±0.5)°C, respectively. The corresponding minimum internal surface temperatures of the three units are about (26.6±0.5)°C, (20.2±0.5)°C, and (25.5±0.5)°C, respectively.

The distributions of temperature differences are illustrated in Fig. 6. The unit averaged temperature differences for the three units are about (6.4 ± 0.7)°C, (4.2 ± 0.7)°C, and (4.4 ± 0.7)°C, respectively. The temperature differences of the door show that the temperature difference is smaller in the higher conductivity single layer glass part of the door, which is colored in yellow compared to the red color dominating the major part of the board of the door.

During the working period from 7:30 to 18:00 of the day, the transient temperature difference distributions for three sample units are plotted in Fig. 7. As shown in Fig. 7, the temperature differences increase in the morning and decrease in the afternoon, due to the sunrise and sunset effects. The maximum temperature difference appears at around 13:30. In addition, the transient temperature differences of the sample units of the door and the wall vary over a wider range of time compared to the changes of the window unit. The reason for this is that the door and wall units have higher thermal resistances than the window unit. The transient distributions of temperature differences obtained is used to calculate the transient sample unit heat flux in the following section.

4.3 Transient heat flux distributions of sample units

Figure 8 plots the transient heat flux distributions for the three units during the working period from 7:30 to 18:00 of the day. As shown in Fig. 8, the transient heat flux values of the three units also increase and decrease according to
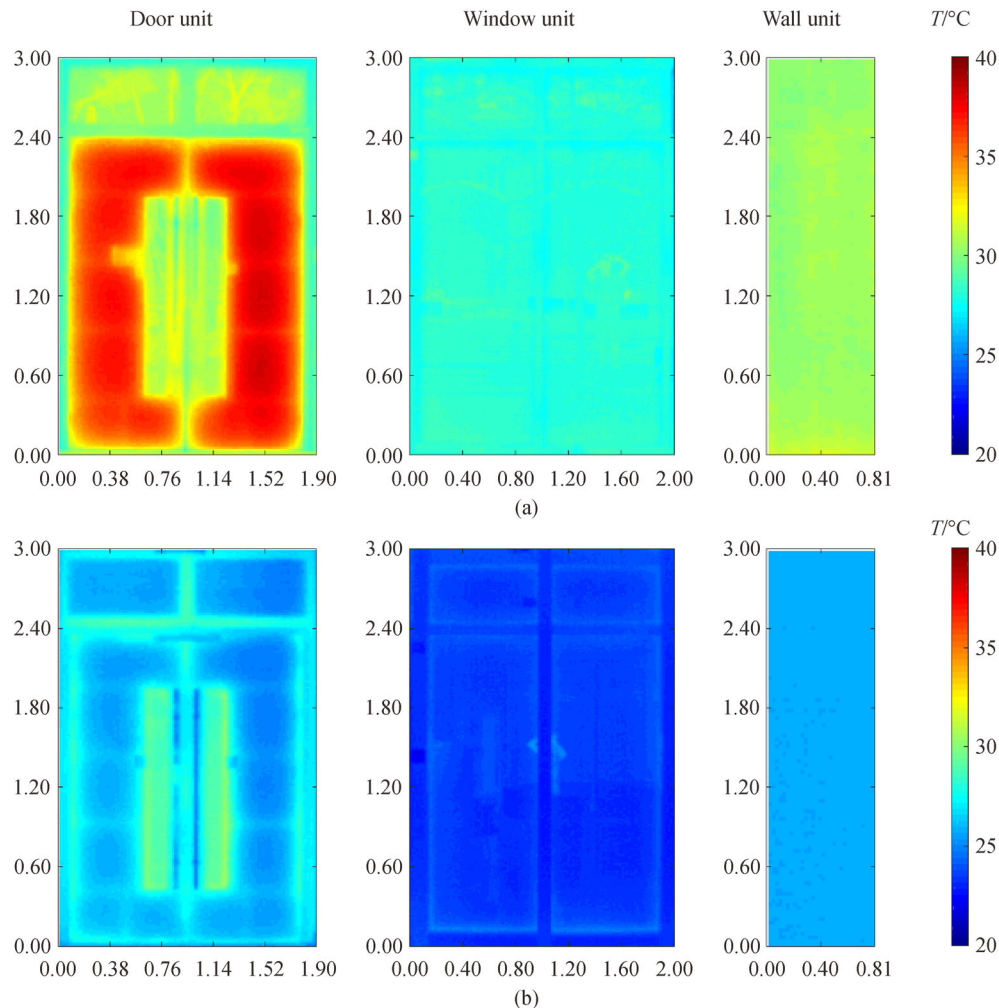

Fig. 5 Contour plots of the outer and inner surface temperatures at noon time of October 19, 2017.
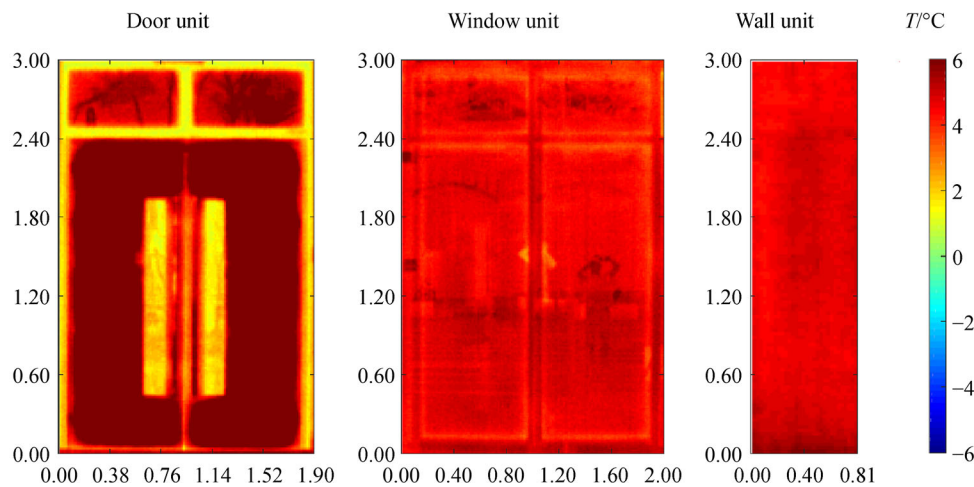(a) External surface temperature; (b) Internal surface temperature.

Fig. 6 Contour plots of temperature difference between the external and internal surfaces at noon time of October 19, 2017.

the sunrise and sunset effects, respectively. For each of the sample unit, the highest heat flux is through the glass parts of doors and windows. The transient heat flux for a sample unit calculated based on Eq. (4) is used to represent the heat flux of that type of unit in the same direction at that time for further integrations of a whole day unit thermal energy leakage value.

4.4 Orientation effects on sample unit heat flux distributions

Now that highest heat flux is through the glass parts, the window units in different orientations are selected to show the effects of orientation directions. The distributions of temperature difference and heat flux for the window units in the four directions on October 19, 2017 are exhibited in Figs. 9 and 10, respectively. As shown in Fig. 9, the south orientated glass window unit has the largest temperature difference at noon, while the west direction oriented glass window has the largest temperature difference at about 13:30. Moreover, it can be seen from Fig. 9 that the temperature differences are not only affected by orientations, but also by the surrounding environmental radiations. The effects of the surrounding environment radiation are more obvious for the north facing window unit shown in Fig. 9. The environment radiation may cause the lower part of the window to get positive heat flux flow into the building, while the upper part the heat flux flow is from the building to the outside environment. This may also be due to the natural convection of the indoor air near the glass window. Figure 10 shows that only the heat flux distributions in the north are similar to the temperature difference distributions. The effect of time on the single layer glass parts is the highest, which are more obviously shown in the east and west directions (shown in Fig. 10). The heat flux distributions are more unevenly distributed compared to temperature difference distributions. Hence,

the present quantitative heat flux distribution based analysis method may provide more accurate building energy leakage surveys compared to direct temperature image observations. Based on the complex transient heat flux distributions of Fig. 10, it can also be expected that the transient energy leakage ratios in the four directions change with direction and time even in a day period.

4.5 Seasonal effects on sample unit heat flux distributions

In order to show the seasonal thermal energy leakage patterns, the temperature difference and heat flux distributions of the three sample units in four seasons are shown in Figs. 11 and 12, respectively. Seasons not only affect the heat flux values but also the heat flux flow directions. It is interesting to observe from Fig. 12 that the heat flux values in spring are the lowest of all the seasons. In spring, the temperature difference is smaller than 2°C, as can be seen from Fig. 11. The transient heat fluxes in spring have both positive (flow into the building) and negative values (flow out of the building). In summer, strong positive heat flux flow are dominating, colored in dark red in Fig. 12. The heat flux in fall is slightly weaker compared to that in summer. In winter, the thermal energy flow is dominated by thermal energy leakage from indoor to outside environment.

Table 2 quantitatively shows the heat flux through one of the three types of sample units for the four seasons. The transient heat flux from different units at various time of a sampling day are integrated by the area of the sample unit, which is also provided in Table 2. The integration of the transient thermal energy transferred for each of the sample unit for the working period of a day is shown in the last column. The uncertainties of the unit heat flux are about 10.5%, 15.3% and 14.8% for door, window and wall units, respectively.

4.6 Seasonal orientation index factors

To further simply the measurements and calibrations of the direction index factors, a constant direction index factor for each direction at each time is expressed as

$$r_{u,d}(t) \approx r_d(t) = \frac{\dot{Q}_{u_{\mathrm{S}},d}(t)}{|\dot{Q}_{u_{\mathrm{S}},d_N}(t_N)|}, \tag{17}$$

and

$$r_{u,d_{\mathrm{S}}}(t) \approx r_{d_{\mathrm{S}}}(t) = \frac{\dot{Q}_{u_{\mathrm{S}},d_{\mathrm{S}}}(t)}{|\dot{Q}_{u_{\mathrm{S}},d_N}(t_N)|}, \tag{18}$$

where u_{S} is the sample unit type. For the sake of simplicity, discussions are limited to the window glass type ($u_{\mathrm{S}} = 2$) because it is more heavily affected by orientations comparing to other units. The daily averaged value for
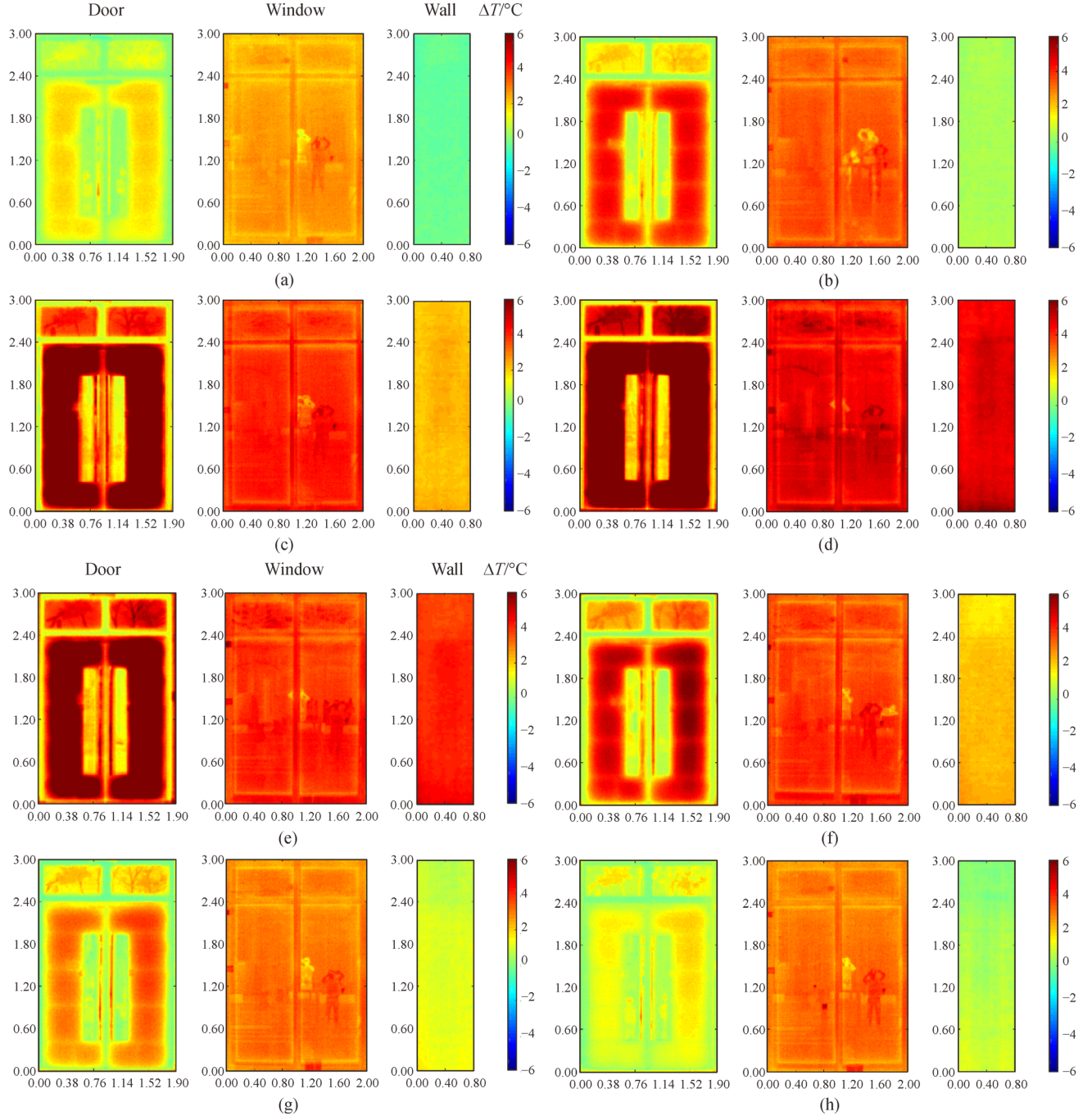

Fig. 7 Transient temperature difference between external and internal surfaces for the three units in October 19, 2017.
(a) $t = 07{:}30$; (b) $t = 09{:}00$; (c) $t = 10{:}30$; (d) $t = 12{:}00$; (e) $t = 13{:}30$; (f) $t = 15{:}00$; (g) $t = 16{:}30$; (h) $t = 18{:}00$.

all directions is approximated by

$$\overline{r}_{u,d} \approx \overline{r}_d = \frac{\displaystyle\int_{t_{\text{start}}}^{t_{\text{off}}} r_d(t)\mathrm{d}t}{\displaystyle\int_{t_{\text{start}}}^{t_{\text{off}}} \mathrm{d}t}. \tag{19}$$

To calculate the energy leakage of all types of units in all directions modeled by Eq. (11), the orientation index factors defined in Eqs. (17) and (18) have to be obtained first. The previous studies on building heat load showed that heat loads of windows change substantially with orientations [31,32]. The orientation index factors are calculated based on transient heat flux and the scaled unit areas, and the top roof orientation index factors are equally weighted by the four directions. The values for all directions and seasons are listed in Table 3. From
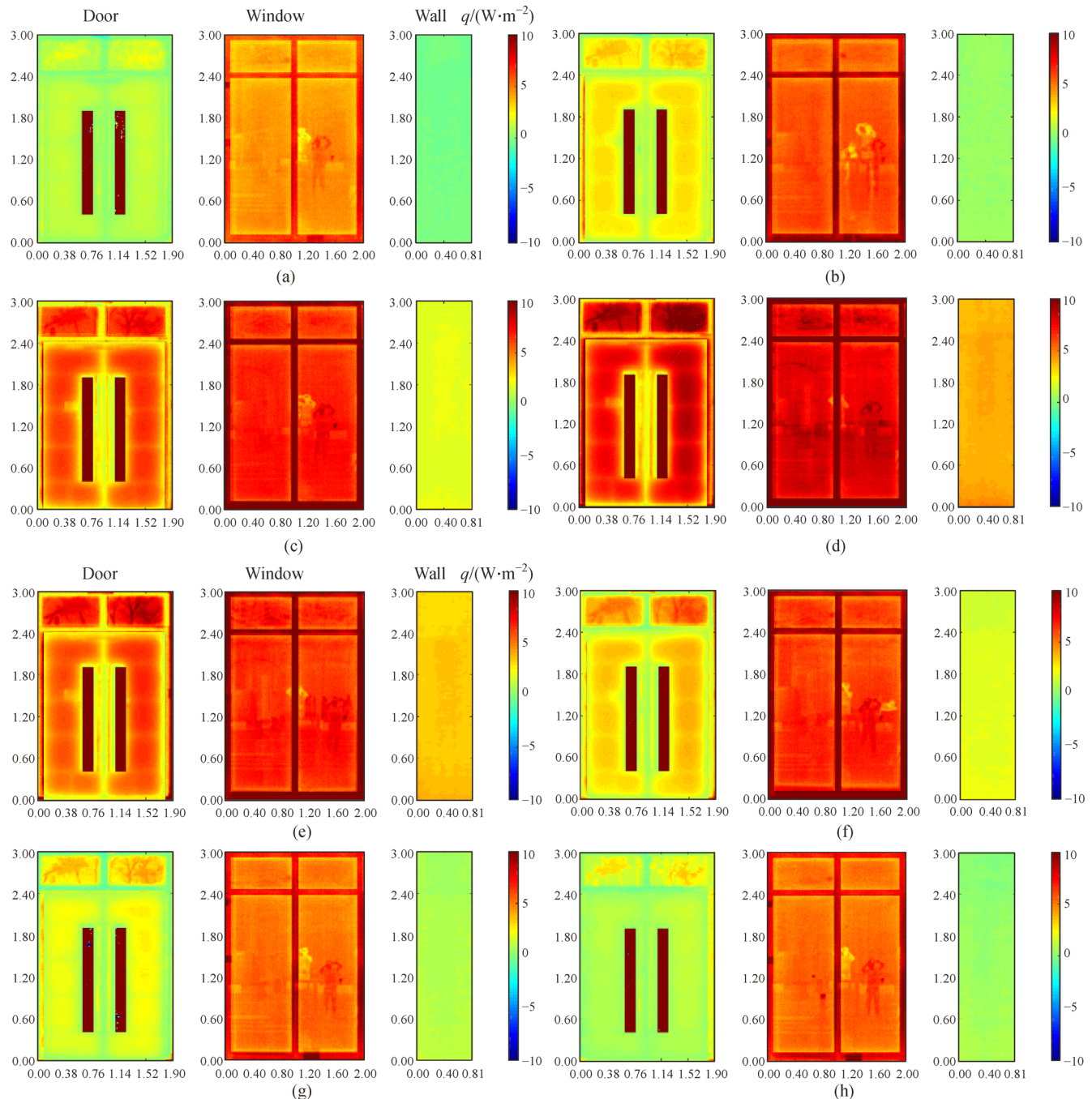

Fig. 8 Transient heat flux between external and internal surfaces for the three units in October 19, 2017.
(a) $t = 07{:}30$; (b) $t = 09{:}00$; (c) $t = 10{:}30$; (d) $t = 12{:}00$; (e) $t = 13{:}30$; (f) $t = 15{:}00$; (g) $t = 16{:}30$; (h) $t = 18{:}00$.

Fig. 9 Transient temperature differences between external and internal surfaces of window units in four orientation directions of October 19, 2017.
(a) $t = 07:30$; (b) $t = 09:00$; (c) $t = 10:30$; (d) $t = 12:00$; (e) $t = 13:30$; (f) $t = 15:00$; (g) $t = 16:30$; (h) $t = 18:00$.
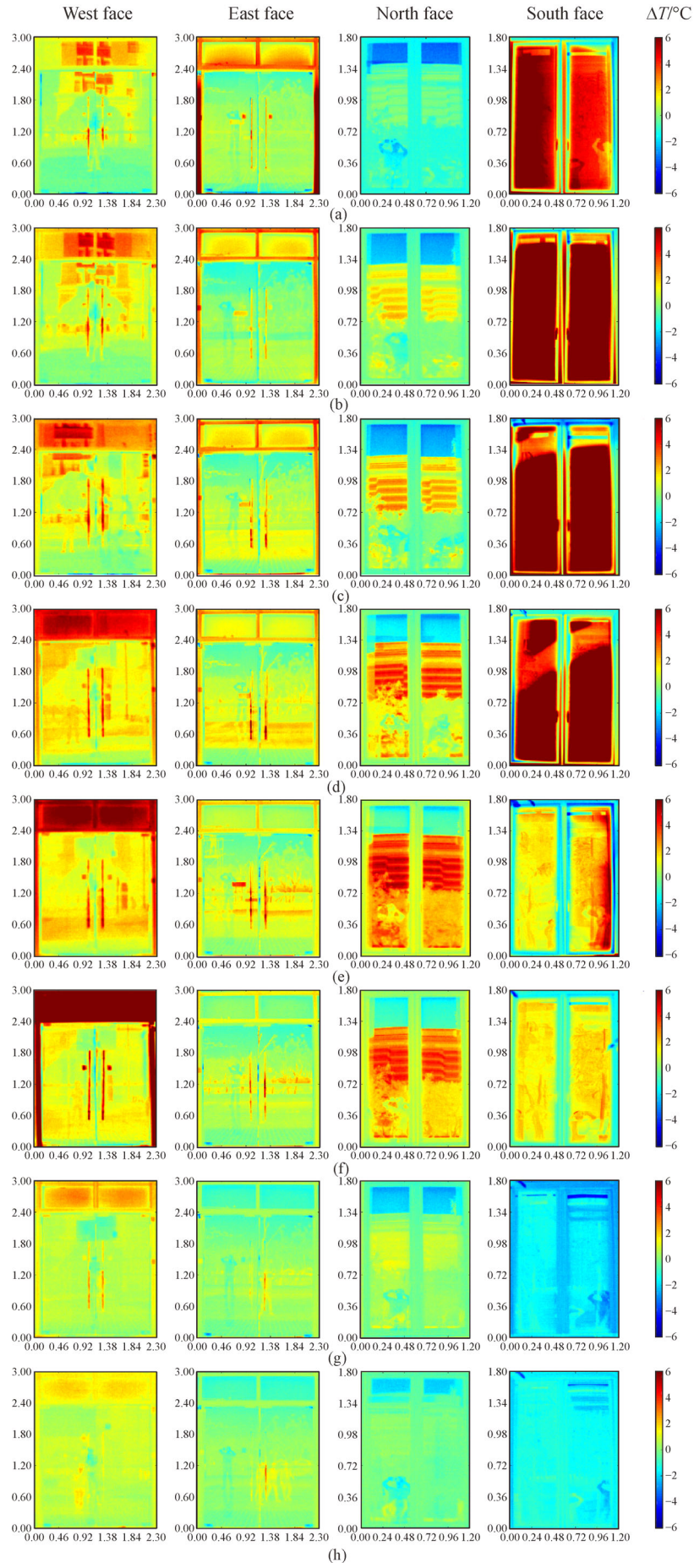
Fig. 10 Transient heat flux between external and internal surfaces of window units in four orientation directions of October 19, 2017. (a) $t = 07:30$; (b) $t = 09:00$; (c) $t = 10:30$; (d) $t = 12:00$; (e) $t = 13:30$; (f) $t = 15:00$; (g) $t = 16:30$; (h) $t = 18:00$.
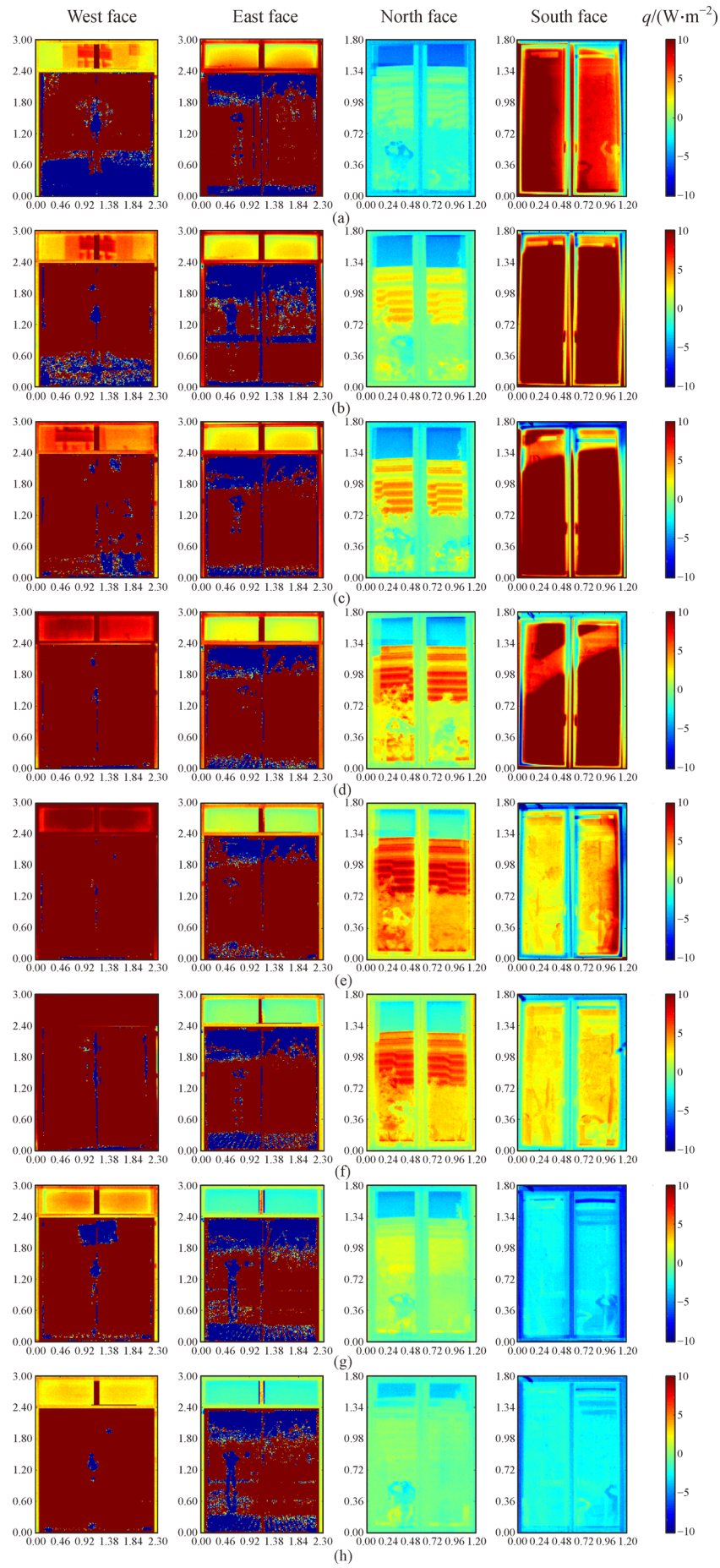
Fig. 11 The seasonal change of the temperature differences between the external and internal surfaces of the three units.
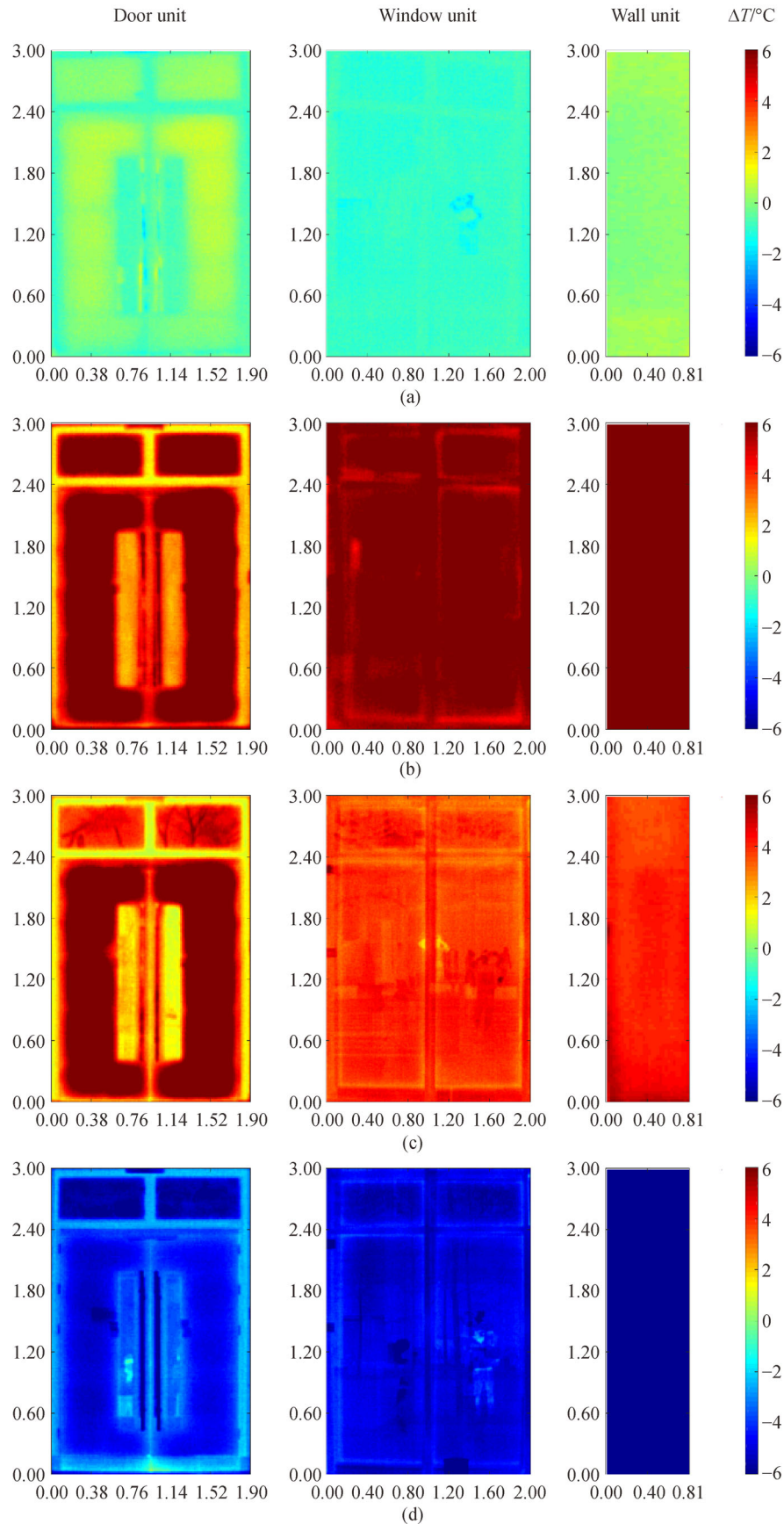(a) Spring (2018-03-06); (b) Summer (2017-07-26); (c) Autumn (2017-10-19); (d) Winter (2018-01-09).

Fig. 12 The seasonal change of the heat flux between the external and internal surfaces of the three units.
(a) Spring (2018-03-06); (b) Summer (2017-07-26); (c) Autumn (2017-10-19); (d) Winter (2018-01-09).
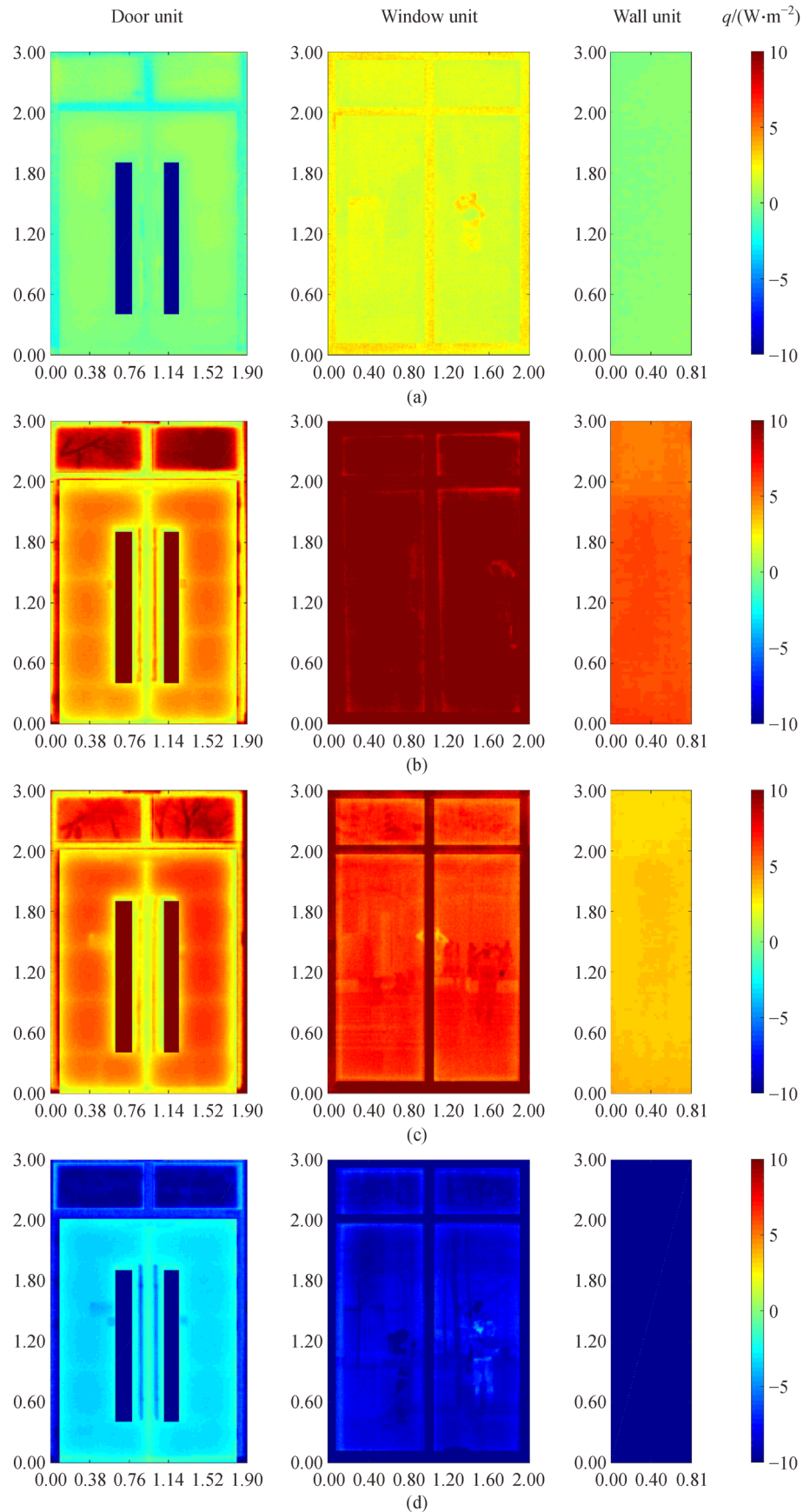
Table 2 Thermal energy leakage from one construction unit in a sample day

Season date	Unit type	d_s	$\dot{Q}_{u,d_s}(t)$ /W								$Q_{u,d_s}(t)$ /kJ
			7:30	9:00	10:30	12:00	13:30	15:00	16:30	18:00	7:30–18:00
Spring 2018/03/06	Door	East	−11.1	16.2	25.6	6.2	5.7	4.9	6.2	−5.9	−304.0
	Window	North	−6.3	−0.7	9.0	12.0	7.6	−6.5	−8.2	−12.4	−21.0
	Wall	South	−4.4	6.4	5.6	7.7	6.4	10.7	−2.6	−6.6	84.6
Summer 2017/07/26	Door	East	115.7	205.5	459.8	200.1	165.0	160.9	156.7	120.7	7918.2
	Window	North	12.3	21.9	49.0	73.6	69.0	61.4	53.7	40.6	1917.4
	Wall	South	12.8	22.7	50.8	33.7	27.6	25.4	23.2	17.4	1071.9
Autumn 2017/10/19	Door	East	41.6	73.9	165.4	209.3	188.5	93.4	53.7	60.4	4510.0
	Window	North	−28.1	37.8	44.5	52.3	43.6	42.0	33.6	−34.2	1202.0
	Wall	South	1.5	1.7	8.0	19.2	16.3	8.6	4.2	1.9	326.8
Winter 2018/01/09	Door	East	−246.7	−315.4	−293.9	−290.6	−310.1	−260.6	−200.9	−190.5	−10206.7
	Window	North	−59.8	−72.1	−70.9	−70.9	−57.0	−62.1	−55.3	−60.0	−2419.9
	Wall	South	−23.1	−26.4	−25.7	−24.1	−26.4	−23.7	−23.4	−21.6	−929.1

Table 3 Thermal energy transport orientation index factors

Season	Orientation	$r_d(t)$								$\bar{r}_d$
		7:30	9:00	10:30	12:00	13:30	15:00	16:30	18:00	
Spring	West	−0.083	−0.015	0.256	0.530	0.808	1.232	−0.164	−0.207	0.358
	East	−0.730	1.067	3.369	0.818	0.744	0.642	0.822	−0.777	0.958
	North	−0.835	−0.086	1.190	1.573	1.000	−0.852	−1.078	−1.635	0.073
	South	−0.584	0.837	0.734	1.011	1.672	1.410	−0.338	−0.866	0.657
	Top	−0.558	0.451	1.387	0.983	1.056	0.608	−0.189	−0.871	0.512
Summer	West	0.603	1.071	2.397	1.517	2.732	2.707	2.333	1.313	1.959
	East	0.839	1.489	3.332	1.450	1.196	1.166	1.136	0.875	1.518
	North	0.179	0.318	0.711	1.067	1.000	0.889	0.778	0.588	0.735
	South	0.741	1.317	2.945	1.956	1.600	1.471	1.342	1.010	1.644
	Top	0.591	1.049	2.346	1.497	1.632	1.558	1.397	0.947	1.464
Autumn	West	0.398	0.698	0.862	1.347	1.616	2.313	0.608	0.507	1.128
	East	0.503	0.893	1.997	1.264	1.138	0.564	0.324	0.365	0.945
	North	−0.645	0.867	1.021	1.200	1.000	0.963	0.771	−0.785	0.730
	South	0.991	1.186	1.672	1.297	1.955	1.734	1.076	0.801	1.402
	Top	0.312	0.911	1.388	1.277	1.427	1.393	0.695	0.222	1.051
Winter	West	−0.836	−0.838	−1.083	−0.943	−0.825	−0.566	−0.648	−0.432	−0.791
	East	−0.817	−1.045	−0.649	−0.642	−0.685	−0.863	−0.666	−0.631	−0.753
	North	−1.050	−1.265	−1.245	−1.244	−1.000	−1.090	−0.970	−1.052	−1.124
	South	−0.464	−0.530	−0.516	−0.485	−0.530	−0.476	−0.470	−0.433	−0.494
	Top	−0.792	−0.919	−0.873	−0.828	−0.760	−0.749	−0.688	−0.637	−0.790

Table 3, it can be observed that the orientation index factors not only change with orientations, but also change with seasons. Besides, the uncertainties of the index factors differ with different unit types. Observed from Table 3, $\delta r_{u,d}/r_d$ are about 14.8%, 21.6% and 21.0% for door, window and wall units, respectively.

4.7 Energy leakage of the whole building

After getting the orientation index, the thermal energy leakage for each unit type in all directions and the whole building are then calculated based on Eqs. (11) and (15). Table 4 lists the total daily energy leakage of the building

Table 4 Total daily energy leakage of the building in the four seasons

Season	Orientation	Unit	Q_{u,d_s}/kJ 7:30 – 18:00	$N_d\bar{r}_dQ_{u,d_s}$//kJ 7:30 – 18:00	$Q_{\text{B,Day}}$/kWh 7:30 – 18:00	$Q_{\text{Ball,Day}}$/kWh	$\hat{E}_{\text{Ball,Day}}$/kWh
Spring	West	Door	113.4	1248			
	East	Door	304.0	2432			
	North	Door	23.2	116			
	South	Door	208.6	417			
	West	Window	102.7	16432			
	East	Window	275.2	48443			
	North	Window	21.0	4228	111.6	122.0	113.0
	South	Window	188.8	48714	±16.9	±18.0	±16.6
	West	Wall	46.0	10313			
	East	Wall	123.4	33932			
	North	Wall	9.4	1858			
	South	Wall	84.6	12020			
	Top	Roof	65.9	221739			
Summer	West	Door	10220.5	112425			
	East	Door	7918.2	63346			
	North	Door	3834.8	19174			
	South	Door	8574.8	17150			
	West	Window	5110.2	817,639			
	East	Window	3959.1	696804			
	North	Window	1917.4	385397	2010.1	2290.1	2120.4
	South	Window	4287.4	1106149	±259.7	±293.6	±271.9
	West	Wall	1277.6	286174			
	East	Wall	989.8	273189			
	North	Wall	479.3	94432			
	South	Wall	1071.9	152203			
	Top	Roof	954.6	3213300			
Autumn	West	Door	5383.7	59221			
	East	Door	4510.0	36079			
	North	Door	3482.7	17414			
	South	Door	6693.5	13387			
	West	Window	1858.0	297287			
	East	Window	1556.5	273940			
	North	Window	1202.0	241595	710.8	845.7	783.1
	South	Window	2310.1	596003	±81.6	±104.7	±96.9
	West	Wall	262.8	58878			
	East	Wall	220.2	60551			
	North	Wall	170.0	33497			
	South	Wall	326.8	46405			
	Top	Roof	245.0	824558			

(Continued)

Season	Orientation	Unit	Q_{u,d_S}/kJ 7:30 – 18:00	$N_d \bar{r}_d Q_{u,d_S}$//kJ 7:30 – 18:00	$Q_{B,Day}$/kWh 7:30 – 18:00	$Q_{Ball,Day}$/kWh	$\hat{E}_{Ball,Day}$/kWh
Winter	West	Door	− 10718.7	− 117906			
	East	Door	− 10206.7	− 81654			
	North	Door	− 15223.7	− 76118			
	South	Door	− 6689.3	− 13379			
	West	Window	− 1703.8	− 272603			
	East	Window	− 1622.4	− 285540			
	North	Window	− 2419.8	− 486389	− 2190.7	− 2340.7	1182.2
	South	Window	− 1063.3	− 274328	±364.8	±369.9	±186.8
	West	Wall	− 1488.7	− 333466			
	East	Wall	− 1417.6	− 389835			
	North	Wall	− 2114.4	− 416531			
	South	Wall	− 929.1	− 131927			
	Top	Roof	− 1487.4	− 5006677			

in different seasons. From Table 4, it can be seen that the heat flux through the door unit is larger than that of the window or wall unit. However, due to the area ratios of windows and walls, the total thermal energy transferred through the window and wall units are larger than that through the door unit. Hence, reducing the thermal leakage of glass windows is essentially important for energy saving.

The conductive thermal energy across all units in the whole building during the working period in a typical day are (111.6±16.9), (2010.1±259.7), (710.8±81.6), and (–2190.7±364.8) kWh for the four seasons, respectively. Based on the approximation of the air leakage of the door unit $r_{1,al} = 50\%±10\%$ and the window unit $r_{2,al} = 30\%± 5\%$, the thermal energy transfer across all units during the working period in a typical day are (122.0±18.0), (2290.1±293.6), (845.7±104.7), and (–2340.7±369.9) kWh for the four seasons, respectively. The incensement is about 10% for the whole building energy leakage, due to the air flow of opening of doors and windows. The absolute values of the thermal energy leakage are considerably large in summer. The corresponding electrical energy consumptions in the four seasons are (113.0±16.6), (2120.4±271.9), (783.1±96.9), and (1182.2±186.8) kWh, respectively, given the approximated pump system efficiency of 90%, and air conditioning system COPs of 1.2 and 2.2 for refrigerator cycle and heat pump cycle.

According to the electrical meter records, the real electrical energy consumption for the air conditioning system in a whole day (including night time ventilation consumption) in summer and winter are about 2450 kWh and 1250 kWh, respectively. Hence, the differences between the predicted electrical energy consumption and the meter value for summer and winter are 13.4% and 5.4%, respectively. These electrical records have validated the present seasonal unit decomposition energy leakage model. The results also show that although the thermal energy leakage level is similar in summer and winter seasons, the consumed electrical energy differs to a great extent, due to the COP difference of the refrigerator cycle and the heat pump cycle. The typical daily thermal energy leakage in winter is the highest, however, the daily air conditioning consumed electrical energy in summer and autumn is higher than that in winter, due to the lower COP of refrigerator cycle compared to the COP of the heat pump cycle of the air conditioning system.

5 Conclusions

Thermography images of both external and internal surfaces of an office building are taken simultaneously by the IRT camera. Besides, the transient local temperature differences are obtained based on the two-side thermography image data analysis with global and local coordinate transformation. In addition, the local effective thermal resistance distributions are calculated by using the porous medium model. Moreover, the transient temperature difference and heat flux distributions for each type of units are clearly demonstrated. Furthermore, the effects of orientations and seasons are indexed by transient orientation index factors for all directions and four seasons, and the effects of the air conditioning system COPs due to different running cycles of refrigerator or heat pump cycles are also considered.

The results show that the values of the conductive thermal flux across all units during the working period in a typical day in the whole building are (111.6±16.9),

(2010.1±259.7), (710.8±81.6), and (−2190.7±364.8) kWh from spring to winter seasons, respectively. With the approximation of the air leakage, the values including both conductive and convective thermal flux are (122.0±18.0), (2290.1±293.6), (845.7±104.7) and (−2340.7±369.9) kWh for the four seasons, respectively. The increment is about 10% for the whole building energy leakage, due to the air flow of opening of doors and windows. The corresponding electrical energy consumptions are (113.0±16.6), (2120.4±271.9), (783.1±96.9), and (1182.2±186.8) kWh for the four seasons, respectively. The typical daily thermal energy leakage value in winter is the highest, however, the daily electrical energy consumption by the air conditioning system in summer and autumn is higher than that in winter, due to the lower COP of refrigerator cycle compared to the COP of the heat pump cycle of the air conditioning system. The results obtained from the present thermography image analysis agree with the electrical meter records, with differences less than 13.4% and 5.4% for summer and winter seasons, respectively. The present model provides a more practical and precise image analysis methods for the thermal energy leakage calculations, and it is suitable for applications in both building historical surveys and new design evaluations.

Notations

A	Heat transfer area/m^2
COP	Coefficient of performance
E	Electrical energy/J
k	Heat conductivity/(W·(m·K)$^{-1}$)
P	Electrical power/W
$\dot{q}$	Heat flux per unit area/(W·m^{-2})
$\dot{Q}$	Heat flux/W
Q	Thermal energy transported/J
r	Orientation index factor
r	Time averaged orientation index factor
R	Thermal resistance per unit area/(m^2·K·W^{-1})
t	Time/s
T	Temperature/K
U	Heat transfer coefficient/(W·(m^2·K)$^{-1}$)

Greek symbols

ΔT	Temperature difference/K
η_p	Pump system efficiency
ϕ	Pore volume fraction Subscripts

Subscripts

B	Total value for a building
d	Orientation index
Day	A day value
k	Number index
layer	The material layer
max	Max number
S	Sample
u	Unit type index

Superscripts

–	Time averaged value

References

1. Bagavathiappan S, Lahiri B B, Saravanan T, Philip J, Jayakumar T. Infrared thermography for condition monitoring: a review. Infrared Physics & Technology, 2013, 60: 35–55

2. Usamentiaga R, Venegas P, Guerediaga J, Vega L, Molleda J, Bulnes F G. Infrared thermography for temperature: measurement and non-destructive testing. Sensors (Basel), 2014, 14(7): 12305–12348

3. Silva N C M, Castro H A, Carvalho L C, Chaves É C L, Ruela L O, Iunes D H. Reliability of infrared thermography images in the analysis of the plantar surface temperature in diabetes mellitus. Journal of Chiropractic Medicine, 2018, 17(1): 30–35

4. Kylili A, Fokaides P A, Christou P, Kalogirou S A. Infrared thermography (IRT) applications for building diagnostics: a review. Applied Energy, 2014, 134: 531–549

5. Lucchi E. Applications of the infrared thermography in the energy audit of buildings: a review. Renewable & Sustainable Energy Reviews, 2018, 82: 3077–3090

6. Garde F, Adelard L, Boyer H, Rat C. Implementation and experimental survey of passive design specifications used in new low-cost housing under tropical climates. Energy and Building, 2004, 36(4): 353–366

7. Barreira E, Almeida R M S F, Delgado J M P Q. Infrared thermography for assessing moisture related phenomena in building components. Construction & Building Materials, 2016, 110: 251–269

8. Albatici R, Tonelli A M, Chiogna M. A comprehensive experimental approach for the validation of quantitative infrared thermography in the evaluation of building thermal transmittance. Applied Energy, 2015, 141: 218–228

9. Li D, Menassa C C, Kamat R. Non-intrusive interpretation of human thermal comfort through analysis of facial infrared thermography. Energy and Building, 2018, 176: 246–261

10. Fox M, Goodhew S, De Wilde P. Building defect detection: external versus internal thermography. Building and Environment, 2016, 105: 317–331

11. Kirimtat A, Krejcar O. A review of infrared thermography for the investigation of building envelopes: advances and prospects. Energy and Building, 2018, 176: 390–406

12. Martín Ocaña S, Cañas Guerrero I, González Requena I. Thermo-

graphic survey of two rural buildings in Spain. Energy and Building, 2004, 36(6): 515–523

13. González-Aguilera D, Lagüela S, Rodríguez-Gonzálvez P, Hernández-López D. Image-based thermographic modeling for assessing energy efficiency of buildings facades. Energy and Building, 2013, 65: 29–36

14. Zalewski L, Lassue S, Rousse D, Boukhalfa K. Experimental and numerical characterization of thermal bridges in prefabricated building walls. Energy Convection and Management, 2010, 51 (12): 2869–2877

15. Asdrubali F, Baldinelli G, Bianchi F. A quantitative methodology to evaluate thermal bridges in buildings. Applied Energy, 2012, 97: 365–373

16. Fokaides P A, Kalogirou S A. Application of infrared thermography for the determination of the overall heat transfer coefficient (U-value) in building envelopes. Applied Energy, 2011, 88(12): 4358–4365

17. Tejedor B, Casals M, Gangolells M, Roca X. Quantitative internal infrared thermography for determining in-situ thermal behaviour of facades. Energy and Building, 2017, 151: 187–197

18. Lehmann B, Ghazi Wakili K, Frank T, Vera Collado B, Tanner C. Effects of individual climatic parameters on the infrared thermography of buildings. Applied Energy, 2013, 110: 29–43

19. Nardi I, Paoletti D, Ambrosini D, de Rubeis T, Sfarra S. U-value assessment by infrared thermography: a comparison of different calculation methods in a Guarded Hot Box. Energy and Building, 2016, 122: 211–221

20. Tran Q H, Huh J W, Kang C H, Lee B Y, Kim I T, Ahn J H. Detectability of subsurface defects with different width-to-depth ratios in concrete structures using pulsed thermography. Journal of Nondestructive Evaluation, 2018, 37(2): 32

21. Rasooli A, Itard L, Ferreira C I. A response factor-based method for the rapid in-situ determination of wall's thermal resistance in existing buildings. Energy and Building, 2016, 119: 51–61

22. Serra C, Tadeu A, Simões N. Heat transfer modeling using analytical solutions for infrared thermography applications in multilayered buildings systems. International Journal of Heat and Mass Transfer, 2017, 115(part B): 471–478

23. Hiasa S, Birgul R, Catbas F N.Investigation of effective utilitzation of infrared thermography (IRT) through advanced finite element modeling. Construction & Building Materials, 2017, 150: 295–309

24. O'Grady M, Lechowska A A, Harte A M. Quantification of heat losses through building envelope thermal bridges influenced by wind velocity using the outdoor infrared thermography technique. Applied Energy, 2017, 208: 1038–1052

25. Baldinelli G, Bianchi F, Rotili A, Costarelli D, Seracini M, Vinti G, Asdrubali F, Evangelisti L. A model for the improvement of thermal bridges quantitative assessment by infrared thermography. Applied Energy, 2018, 211: 854–864

26. Bentz D P, Peltz M A, Dur'an-Herrera A, Valdez P, Ju'arez C A. Thermal properties of high-volume fly ash mortars and concretes. Journal of Building Physics, 2011, 34(3): 263–275

27. Javadi H, Mousavi Ajarostaghi S, Rosen M, Pourfallah M. A comprehensive review of backfill materials and their effects on ground heat exchanger performance. Sustainability, 2018, 10(12): 4486

28. Jalilluddin A M, Ayop S M, Kamaruddin K. Evaluation on the thermal conductivity of sand-cement blocks with Kenaf Fiber. Advanced Materials Research, 2012, 626: 485–489

29. Gandage A S, Rao V R V, Sivakumar M V N, Vasan A, Venu M, Yaswanth A B. Effect of perlite on thermal conductivity of self-compacting concrete. Procedia: Social and Behavioral Sciences, 2013, 104: 188–197

30. Menezes A C, Cripps A, Buswell R A, Wright J, Bouchlaghem D. Estimating the energy consumption and power demand of small power equipment in office buildings. Energy and Building, 2014, 75: 199–209

31. Rawat V, Shivankar S, Das B, Sil B. Effect of orientation of window on building heat load: perspective of N-E India. Materials Science and Engineering, 2017, 225: 012166

32. Vanhoutteghem L, Skarning G C J, Hviid C A, Svendsen S. Impact of facade window design on energy, day lighting and thermal comfort in nearly zero-energy houses. Energy and Building, 2015, 102: 149–156